UAV-LIDAR BORESIGHT ESTIMATION USING VIRTUAL CONTROL POINTS: A CASE STUDY

M. V. Machado [1], A.M.G. Tommaselli [1] *

[1] São Paulo State University, Presidente Prudente, SP, Brazil, {marcela.machado, a.tommaselli}@unesp.br

KEY WORDS: UAV-lidar systems, boresight misalignment, least squares methods, point-to-point approach, virtual control point.

ABSTRACT:

UAV-lightweight systems can achieve centimetric accuracy, being a viable alternative for forestry mapping and agriculture. However, they are smaller and more flexible systems, making them more susceptible to error influences than conventional systems. The errors from misalignment between the inertial measurement unit (IMU) and the laser unit, scanning angles, ranges, and the identification of interest features can significantly affect the accuracy of the point cloud. This paper aims to compare two different stochastic models using system raw data for boresight misalignment. Furthermore, to minimise the error in identifying the control point in the point cloud, a technique to create virtual control points is proposed and analysed. These strategies were tested with real flight data, and no significant differences were observed between the two mathematical models in the experiments performed in this study. However, the technique of virtual points enabled an improvement of 13.84% in the results. The accuracy achieved for the point cloud was close to 19 cm in planimetry and 10 cm in altimetry.

1. INTRODUCTION

Lightweight laser scanning systems on board Unmanned Aerial Vehicles (UAV) have become widely used in different applications, such as forest mapping (Jaakkola et al., 2010; Wallace et al., 2012; Torres and Tommaselli, 2018) and agriculture management (Elbahnasawy et al., 2018). There are several manufacturers integrating commercial systems (Riegl, 2023; YellowScan, 2023; Stroner et al., 2021). These systems usually integrate small laser scanning and direct georeferencing units, which measure range, scan mirror angles, position and orientation, respectively (Jaakkola et al., 2010). Combining the measurements provided by these sensors and applying corrections from mounting parameters (boresight angles and lever-arm offset) results in a laser point cloud.

The accuracy of the generated ground point is dependent on random and systematic errors. The errors caused by navigation solution (errors in position and attitude of the sensor platform), laser scanning (scan angle, range measurement, effect of footprint size) involve random and deterministic components. In addition, systematic errors are also caused by boresight misalignment, lever-arm offset, time synchronisation and terrain characteristics (May, 2008).

Modelling systematic errors in lightweight systems on board UAVs can be more challenging than conventional Airborne Laser Systems (ALS). Important issues are the low spatial sampling and few return pulses from the laser unit, which affect the identification of control entities. Additionally, the accuracy of the navigation system is usually lower, mainly due to IMU errors. The errors from external factors associated with platform instability in windy conditions, ground and object characteristics can also affect the collected data. The angular misalignment between systems, which significantly affects the overlap strips, becomes one of the primary error sources to be determined through a calibration procedure based on indirect observations. The lever arm offsets are usually measured directly with high accuracy.

Several calibration approaches were developed to model and correct systematic errors in conventional ALS systems. Examples are strip adjustment methods, which are based on the reduction of discrepancies between overlapping strips using the coordinates of the point clouds (Habib et al., 2010). Calibration with emphasis on the system data, on the other hand, relates measurements and parameters of the system with ground points' coordinates through the sensor's physical model, mainly considering the nature of the data available, such as flight trajectory, time tag data or raw system data (Habib et al., 2010). When the raw data is available, the calibration becomes more rigorous since more error sources can be minimised during the estimation process (Habib et al., 2010). Mounting parameters are often estimated with a conventional Least Squares Method (LSM) based on linearised observation Equations (Gauss-Legendre model) (Filin, 2003; Friess, 2006; Kersting and Habib. 2012) or with a more rigorous approach based on combined method (Gauss-Helmert solution) (Skaloud and Litchi, 2006; May and Toth, 2007). Moreover, calibration methods can also be associated with different control primitives, which can be points, lines, or planes, the last being often used and in commercial solutions (Schneider, 2009). However, plane-based approaches may not be suitable for all types of practical situations (Filin, 2003), requiring natural flat surfaces, which are not found in agricultural and forest areas, for instance. In these areas, techniques based on artificial targets are more common (Ravi et al., 2018).

Some research works (Jaakkola et al., 2010; Wallace et al.,2012; Torres and Tommaselli, 2018) have used lightweight systems, such as the Ibeo LUX laser scanner. They concluded that the calibration of this type of system is troublesome, mainly the indirect determination of boresight misalignment errors. Jaakkola et al. (2010) and Wallace et al. (2012) considered that the boresight calibration could even be neglected in their study cases because both the angular resolution (0.25°) and altimetric accuracy (10 cm) of the positioning and orientation system were lower than the expected accuracy for the whole systems. Torres and Tommaselli (2018) presented an in-situ boresight calibration technique based on control points. The low number of returns

* Corresponding author

from the IbeoLUX laser and the point cloud density became difficult to identify points and common features in the point cloud with suitable distribution and accuracy. The low density of the point cloud associated with the absence of intensity data and a single flight height resulted in a high standard deviation for estimated boresight angles in that study. The calibration of different lightweight systems (Velodyne VLP-16 Puck HI-RES laser scanner) using a plane-based approach can be found in Shamseldin et al. (2018) and Oliveira Jr and Santos (2019). However, the use of those approaches requiring man-made features (regular lines or planes) in on-the-job calibration is limited to specific areas such as urban environments.

This paper presents a study case of an in-situ calibration approach using raw data from a lightweight laser scanning system, focusing on the estimation of boresight misalignment. Two mathematical models for the stochastic treatment of the laser data are implemented and analysed. A Virtual Control Point (VCP) technique is also used to reduce the measurement errors of the point-to-point approach since some applications, such as agriculture and forests, require signalised control points.

2. UAV LASER SCANNING SYSTEM

A UAV-based mapping system used in this research is composed of an Ibeo LUX laser scanner unit, model 2010, (Figure 1.a), an integrated inertial navigation system GNSS/IMU SPAN–IGM–S1 (Figure 1.b) and two microcomputers Raspberry Pi 3 (Figure 1.c). This system is loaded by the UX4 quadricopter (Figure 1.d), which carries a payload of approximately 2,5 kg.

Figure 1. Laser Scanning System: (a) Ibeo LUX, (b) SPAN-IGM-S1; (c) Raspberry Pi 3; (d) Final payload assembled with a UAV quadrocopter.

The Ibeo LUX laser unit was chosen due to its range limits varying from 0.3 to 200 m, compact size and low weight, which is important when carrying it aboard a UAV. The nominal accuracy is close to 0.04 m, with a data rate of 25 Hz. A horizontal field of view of 60º (30º to -30º) is used in the Ibeo LUX as well as a fixed vertical field of view of 3.2º (+1.6º to -1.6º) Machado (2019). According to Torres and Tommaselli (2018), the laser unit operation is based on two emitters and four receivers, which generate four scan levels. These levels are generated by four receivers, two of them receiving pulses simultaneously and used to generate the scan lines. Each complete scan turn generates a data package composed of point identification (point ID), scan level (1,2,3,4), pulse return number (echo), vertical angle (in radians), horizontal angle (in radians), distance (m) and pulse width (cm), in addition to the start and the end time of each complete mirror scan (given in the laser time system).

Platform position and attitude is provided by the Novatel SPAN–IGM–S1 unit, which integrates a dual-frequency GNSS receiver and a STIM300 IMU with 3 gyroscopes and 3 accelerometers. This IMU collects data at a rate of 125 Hz and the GNSS at 20 Hz. The horizontal and vertical positional accuracy is around 0.02 m and 0.03 m, respectively. The attitude accuracy is around 0.015° for roll and pitch angles and 0.08° for heading angle. These results are obtained in a post-processing mode (NovAtel, 2014). The Raspberry Pi 3 computers are used to collect the data of each sensor independently. Time synchronisation of the laser is provided by GNSS PPP (pulses per second) mode and NMEA messages.

The classic point-positioning Equation (1) relates the measurements derived by each system component (El-Sheimy et al., 2005, adapted by Torres and Tommaselli, 2018) with the resulting 3D ground coordinates.

$$r_i^g = r_{GNSS}^g(t) + R_{IMU}^g(t) r_{LU}^{IMU} + R_{IMU}^g(t) R_{LU}^{IMU} R_{ED}^{LU}(t) \rho_I \quad (1)$$

According to Habib et al. (2010), the main elements of Equation 1 are: the vector of ground coordinates of point *i* (r_i^g); the vector of the ground coordinates of the GNSS antenna at instant *t*, reduced to the geodetic reference system ($r_{GNSS}^g(t)$); the rotation matrix, relating the ground and IMU coordinate systems at instant *t*, derived after processing the GNSS and IMU data ($R_{IMU}^g(t)$); the vector of offsets between the laser unit and the IMU origin (lever-arm - r_{LU}^{IMU}); the rotation matrix relating the laser unit coordinates system and the laser emitting devices (mirror scans angles) at instant *t* (R_{ED}^{LU}); the vector of the coordinates of point *i*, stated in the emitting device (ED) reference system (ρ_i). The rotation matrix relating the laser unit and IMU coordinate system is expressed as a function of the approximate angles directly measured, also known as the boresight angle matrix ($\Delta\kappa$, $\Delta\varphi$, $\Delta\omega$) (R_{LU}^{IMU}). The laser unit used in this research scans four horizontal layers, and thus, the rotation matrix is expressed as a function of angles β and θ) (R_{ED}^{LU}).

3. BORESIGHT ESTIMATION TECHNIQUES

3.1 The Mathematical Models and Least Squares Methods

This section presents two different techniques to estimate boresight misalignment angles based on raw data and a point-to-point approach, including a technique of Virtual Control Points (VCPs). These techniques of boresight determination are based on the laser mathematical model as presented in Equation (1) and rearranged to obtain Equation (2), which is written for each control point and used with Least Squares Method (LSM). A second option is to use Equation (5), which requires a combined model for parameter estimation, also known as Gauss-Helmert model (Wells and Krakiwsky, 1971).

In Equation (2), the left side denotes the Ground Control Point (GCP) coordinates transformed to the laser reference system using the position and orientation data of the platform. On the right side of the Equation, there are the coordinates of this point measured by the laser unit. The rotational differences between these systems are the unknown angular misalignment, which must be estimated indirectly. The estimation of these angular misalignments, it is required to generate an initial point cloud to identify the GCPs. Each point in the points cloud is associated with a time tag and a raw dataset from the laser file and the

GNSS/IMU data. A point closest to the GCP is manually identified in the point cloud collected in the field, and the time tag associated with the point is used to extract the raw data. These data are then used to determine the angular misalignment, which will be used to correct the initial point cloud after being determined.

$$R_{IMU}^{g}(t)^{-1} * \left[r_i^g - r_{LS}^g(t)\right] = R_B R_{LU}^{IMU} r_i^{LU}(t) \quad (2)$$

Where: r_i^g are the ground coordinates of a point *i*; r_{LS}^g is the vector of coordinates of the centre of the laser unit in the geodetic reference, given by Equation (3); $r_i^{LU}(t)$ is the vector of coordinates of point *i* in the laser unit reference system (Equation 4); R_B is the rotation matrix as a function of the unknown parameters (boresights angles - $\Delta\omega, \Delta\varphi\ e\ \Delta k$). The elements of rotation matrix R_{LU}^{IMU} are known as: $\kappa = 0^o$, $\varphi = -90^o$, and $\omega = 90^o$.

$$r_{LS}^{g} = r_{GNSS}^{g}(t) + R_{IMU}^{g}(t) r_{LU}^{IMU} \quad (3)$$

$$r_i^{LU}(t) = R_{ED}^{LU}(t) \rho_i(t) \quad (4)$$

Each control point generates three equations. The left components of Equation (2) are considered pseudo-observations with the same precision (Torres and Tommaselli, 2018) and the three boresight angles are the unknowns. They can be estimated with the classical Gauss-Legendre LSM, considering the weight matrix as identity and neglecting any other errors, such as errors in the identification and measurement of control point coordinates.

However, errors resulting from the acquisition of these coordinates, errors associated with the scanning angles (vertical and horizontal) and errors in the range measurements remained unmodelled. Thus, a more reliable determination of the boresight angles should consider six observations: coordinates of control points ($X_{GCPi}, Y_{GCPi}, Z_{GCPi}$), scanning angles ($\theta$ and β) and the range (ρ). To cope with this set of observations and parameters, a combined model for parameter estimation with LSM, as described by Wells and Krakiwsky (1971) is used. Rearranging the basic mathematical model presented in Equation (1), leads to Equation (5).

$$R_{IMU}^{g}(t)^{-1} * \left[r_i^g - r_{LS}^g(t)\right] - R_B R_{LU}^{IMU} r_i^{LU}(t) = 0 \quad (5)$$

The three non-linear Equations (5) can be linearised by Taylor expansion and represented with matrices notation as Equation (6). According to Wells and Krakiwsky (1971), *X* are the corrections to the approximate values for the unknowns ($\Delta\omega_i, \Delta\varphi_i, \Delta k_i$), *V* are the observations' residuals, *A* and *B* the matrices of partial derivatives with respect to the parameters and observations, respectively, and *W* a misclosure vector.

$$_{n*3}A_3 * _{n*3}X_1 + _{n*6}B_{n*3} * _{n*3}V_1 + _{n*3}W_1 = 0 \quad (6)$$

The observation vector is composed by $X_{GCPi}, Y_{GCPi}, Z_{GCPi}, \alpha_i, \beta_i, \rho_i$ for each GCP.

Considering independent and uncorrelated observations, covariances can be neglected, and a diagonal weight matrix is generated. The weights of the observations are defined as a ratio of the *a priori* sigma and the variances (σ^2) of $X_{GCPi}, Y_{GCPi}, Z_{GCPi}$ and θ, β, ρ. An iterative process updates the estimated values (Xa) with the corrections calculated in each iteration (Wells and Krakiwsky,1971). Therefore, this model becomes an alternative for determining the boresight angles since it takes into account the uncertainty related to the control points both due to the measurement errors and the identification in the point cloud. Also, different weights can be assigned to the angle's measurement errors.

Both models were implemented as scripts in SCILAB, 6..1.1. In addition to using a more rigorous adjustment to determine boresight angles, the VCP technique was developed to mitigate the measurement error caused by the identification of the GCP in the point cloud, as described in the next section.

3.2 Virtual Control Points

The point cloud used in this paper has an average spacing between points of approximately 0.3 m (density of 11 pts/m²), considering the laser scanning and the flight height used in the experiments, which affects the identification of points of interest in control targets. Therefore, it is necessary to use control targets with suitable shapes and sizes, such as building corners, flat planes or specially designed trapezoidal targets.

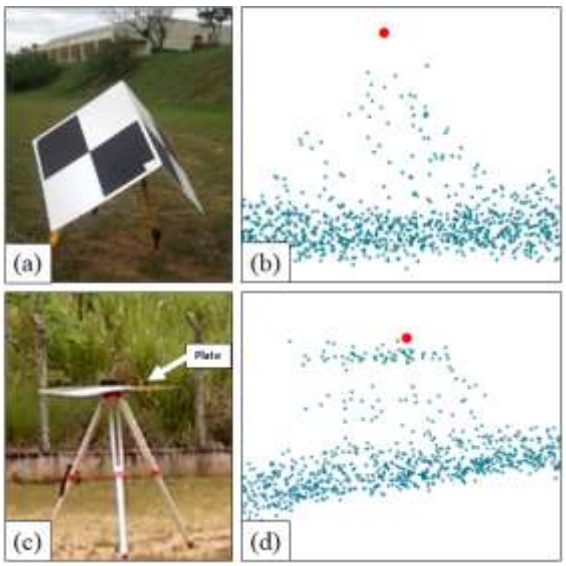

Figure 2. (a) Trapezoidal control target; (b) the point cloud sample (blue) and the control point (red); (c) flat plate control target and (d) the point cloud sample.

The trapezoidal target (Figure 2.a) has been designed and used in this work since it facilitates the identification of apex points in the laser point cloud. The target has three planes (faces measuring 90 cm x 90 cm), and the point of intersection of these planes enables to identify the interest point. A second type of target employed is a horizontal flat plate (Figure 2.c). Using these points in quality control or in determining the boresight misalignment angles requires their identification in the point cloud and the location of a point closest to the apex (trapezoidal target) or the centroid (flat target). However, this point identified in the point cloud will not correspond to the control point measured in the field with a GNSS receiver, and this discrepancy will depend on the point's spacing. Due to the density and noise of the point cloud generated by this laser unit, it was observed that the modelling of the trapezoidal shape (Figure 2.b) was sparser than the flat target (Figure 2.d). Therefore, the point manually identified as closest to the apex point can be too far from the measured GCP.

In Figure 2.d, some non-real points between the flat target and the ground can be seen. These points were most likely generated due to the footprint size since part of the footprint is projected on the plate and another part on the ground or tripod tip. A manual clipping is performed in the Cloud Compare software to

eliminate noisy and ground points around the target. Then, the centroid is determined based on the average of the point's coordinates laying on the plate.

The errors caused by the discrepancies in the coordinates of the point closest to the apex of the trapezoidal target in comparison to the GCP coordinates affect the quality control and the boresight determination. This effect can be mitigated by creating Virtual Control Points (VCP). As shown in Figure 3.a, the top of the trapezoidal target is not well defined in the point cloud, generating errors in identifying the apex point. The alternative is to create a virtual GCP corresponding to the point measured in the laser point cloud.

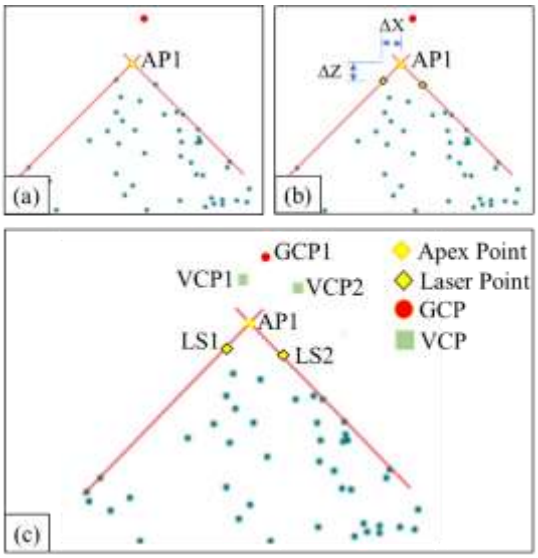

Figure 3. Virtual control point technique: (a) apex point of the target in the laser cloud is generated from the intersection of planes; (b) discrepancies between the apex point and the nearest neighbours are determined, and (c) Virtual Ground Control Points are created.

The first step in the determination of the VCP is the computation of the apex coordinates from the point cloud data, which can be done by fitting three planes to each target and then computing the intersection of these three planes. The points belonging to each plane are selected based on the direction of the normal vectors to each point. Outliers are recursively eliminated based on point-to-plane distance analysis. The point of intersection of the three planes is considered the apex point in the laser point cloud (Figure 3.a.) and is used to calculate the VCP.

The second step is to calculate the discrepancies between the 3D coordinates of the apex points to the nearest neighbour point selected (top point) in the point cloud, as shown in Figure 3.b. The third step is to create the VCPs, which correspond to the nearest neighbours (VCP1 and VCP2 in Figure 3.c.) from the difference between the ground control coordinates (GCP1) and the discrepancies calculated in the previous step. For the same GCP, several VCPs can be generated. Using this concept of VCP, errors related to the identification of points are reduced and better results in boresight estimation and quality control are achieved.

4. EXPERIMENTS AND RESULTS

4.1 Data Acquisition and Processing

The data was acquired with the lightweight system carried by a UAV in an experimental area of São Paulo State University, campus of Presidente Prudente - São Paulo, Brazil, as presented in Figure 4. The flight height was 50 m, and the flight lines were oriented north-south, totalling six strips with a lateral overlap from 60% to 80%. Flight manoeuvres were performed with the system to improve the accuracy of the inertial system's attitude data.

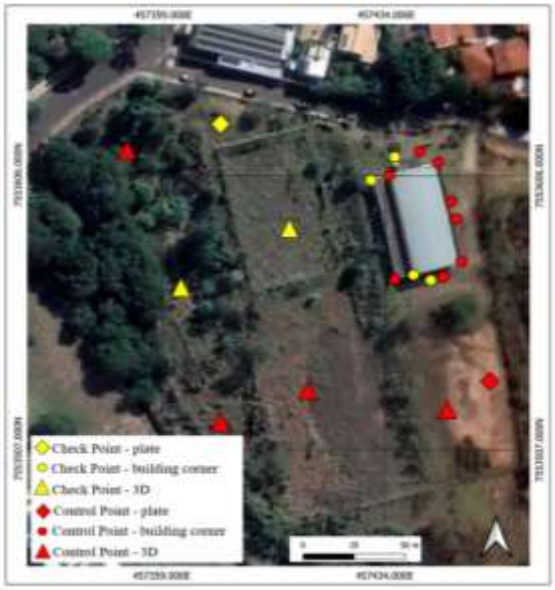

Figure 4. Control and check points distribution at study area to boresight estimation and quality control.

The GNSS and IMU data were processed with Inertial Explorer (NovAtel, version 8.9), achieving average planimetric and altimetry of approximately 0.004 m and 0.007 m, respectively. The attitude angles were obtained with a standard deviation of 0.004° for pitch and roll angles and 0.02° for the heading angle. For the laser scanning data, as the laser unit manufacturer does not specify the standard deviation of the vertical and horizontal angles, it was defined based on the expected errors for this sensor, according to the motor step. One-third of this angular increment was initially applied, which corresponds to 1 arcsec or 4.848137 E-6 rad (0°0'01"). The nominal accuracy of the range measurement is 4 cm, according to the manufacturer. From the determination of the dataset, the laser scanning point cloud was generated based on Equation (1) (Torres and Tommaselli, 2018).

For the boresight estimation and quality control, 20 GCPs were collected in the study area (6 trapezoidal, two flat plates and 12 building corners). From the total of GCPs, 13 points were used as control for boresight estimation (4 trapezoidal, 1 plate and 8 building corners) and the remaining (7) as check points (ChP). The coordinates of the targets were collected using a dual-frequency Hiper GGD GNSS receiver. The GNSS data was processed in the Grafnet software (NovAtel, version 8.9), achieving a positional accuracy of approximately 0.025 m. Figure 4 presents the distribution of the GCPs and ChPs.

4.2 Boresight Estimation and Virtual Control Points

In this paper, a comparative analysis of two least squares approaches for boresight estimation were performed. The use of VCPs was also considered as a strategy to improve the determination of boresight misalignment. The performance of the methods and the final accuracy of the point cloud were assessed in six experiments, which were divided in two groups. In the first group, only the two least squares approaches were analysed. The

second group presented experiments with least squares approaches and VCP technique. Table 1 describes the main features of each experiment.

Experiments	Characteristics	
A	Without boresight correction	***(Group 1)*** *Conventional GCP*
B	Boresight estimation based on Gauss-Legendre solution	
C	Boresight estimation based on Gauss-Helmert solution	
D	Without boresight correction	***(Group 2)*** *Using Virtual Control Point (VCP)*
E	Boresight estimation based on Gauss-Legendre solution	
F	Boresight estimation based on Gauss-Helmert solution	

Table 1. Characteristics of the experiments classified in two groups.

In experiment A, the point cloud was processed and analysed without any correction for the boresight misalignment angles, which made it possible to have the magnitude of the errors in each strip using the GCPs as a reference. The same strategy was adopted in experiment D, but with using VCPs for the quality assessment. In experiments B, C, E and F, four sets of boresight angles were estimated since tests were performed with different adjustment methods and with the VCP technique. The experiments were performed with a homogeneous distribution of GCPs in the study area, and these GCPs are well-defined features in the field, such as building corners and special targets (plates and trapezoids).

In experiment B, the classic Gauss-Legendre adjustment method with observation equations was used, as discussed in Torres and Tommaselli (2018). The standard deviation of the observations was considered to be the same and, thus, the weight matrix is considered to be the identity. In experiment C, the combined method (Gauss-Helmert) was used to give a more rigorous treatment to the stochastic properties of observations and parameters. Therefore, four different observational errors were considered in the adjustment: horizontal scan angle, vertical scan angle, the distance measured by the laser ranging device and measurement errors in the GCPs (X_{GCP}, Y_{GCP}, Z_{GCP}).

As the vertical angle error is very small, the value of 1 arc sec was kept. For the horizontal angle, the error is higher than the vertical angle. Therefore, based on different experiments to estimate boresight angles, the value of 2.42441 E-4 rad (0°0'50.01") was adopted. The projection of this error on the ground, for a height of 50 meters, corresponds to 0.012 m, which was acceptable for this system. The final standard deviations used for each of these observations were: σ_α = 2.42441 E-4 rad, σ_β = 4.848137 E-6 rad, σ_ρ = 0.04 m and σ_{XGCP} = 0.05 m, σ_{YGCP} = 0.05 m and σ_{ZGCP} = 0.10 m.

A total of 19 points were observed in the point clouds and used in the experiments, with some of them appearing in two or more strips but corresponding to the same ground points. The point cloud was calculated with in-house developed software (Torres and Tommaselli, 2018), and the boresight estimation algorithms were implemented as scripts in SCILAB 6.1.1.

To improve the accuracy in the estimation of the boresight angles, experiments E and F were performed with the VCP technique, using the same parameters from the B and C experiments. Only trapezoidal control targets were used in these experiments since plates and building corners did not achieve enough points' density to enable the determination of a virtual point with the expected accuracy. Six trapezoidal points were used in the experiments with the VCP technique. Each Ground Control Point generated a set of virtual ground coordinates, which changed from strip to strip. Thus, using the same virtual control coordinates in different strips was not feasible since the virtual coordinates are valid only for the strip for which it was calculated. Thus, each GCP point had different VCP coordinates depending on the strip. The coordinates of two points were collected (LS1 and LS2, as shown in Figure 3.c.) for each strip. Some experiments were performed, and it was concluded that more than two VCPs for each GCP do not increase accuracy since the VCPs come from the same data.

The average of the residuals for *E*, *N* and *h* components of the observations, are presented in Table 2 after the estimation of the boresight angles. The set of estimated boresight misalignment angles obtained in all experiments and the corresponding standard deviation are presented in Table 3.

	A	B	C	D	E	F
$\bar{x}_E$ (m)	-	-0.157	0.038	-	-0.183	0.042
$\bar{x}_N$ (m)	-	-0.654	0.014	-	-0.699	0.022
$\bar{x}_h$ (m)	-	-0.084	-0.095	-	-0.017	-0.038

Table 2. The average of the residuals after estimation of boresight angles with LSM.

	$\Delta\omega(°) \pm \sigma_\omega(°)$	$\Delta\varphi(°) \pm \sigma_\varphi(°)$	$\Delta\kappa(º) \pm \sigma_\kappa(º)$
A	-	-	-
B	0°45’00”± 0°07'34"	-0°10’34” ± 0°06’32	-0°01’60” ± 0°26'7.6"
C	0°44’41” ± 0°02’33”	-0°10’19” ± 0°02’16”	-0°10’19” ± 0°08’56”
D	-	-	-
E	0°47’53” ± 0°07’59”	-0°12’42” ± 0°06’56”	-0°02’14” ± 0°27’53”
F	0°45’37” ± 0°02’23”	-0°12’47” ± 0°02'07"	-0°19’03” ± 0°08'21"

Table 3. Estimated boresight misalignment angles and estimated standard deviations.

The analysis of the average of residuals by components (Table 2) showed that the largest values occurred with the first method using Gauss-Legendre model, which uses the same weight for all observations. A systematic trend was observed in the residuals of experiments B and E, with larger magnitude in the N component. When applying the Gauss-Helmert method, the distribution of residuals was random, and standard deviations of the angles were smaller, indicating the importance of using suitable weights applied to the observations and a more rigorous stochastic treatment with the combined method (Gauss-Helmert). Thus, improvements were observed when applying the second method (C and F) in relation to the first (B and E), mainly in *kappa* angle. Considering the VCP technique and the residuals, it is possible to verify a small improvement in experiment F in relation to experiment C, regarding the altimetry. In the planimetry, there no significant improvements were observed with the use of VCPs.

4.3 Assessment of the Point Cloud Accuracy

Accuracy assessment is an important step to verify whether the generated point cloud can be used to extract reliable variables for forestry or agricultural mapping and to analyse the performance of estimation methods with VCPs. According to Ojoatre et al. (2019), tree height and crown diameter are parameters that can be obtained with laser scanning data. Measurements obtained with hypsometers, the equipment commonly used to measure the

height of trees, were compared with data from ALS (with 10 cm point accuracy), and a RMSE of 3.11 m was achieved. These results showed that airborne laser scanning is more accurate than existing techniques for the forestry application mentioned by the authors.

Thus, quality control was divided into two steps: internal control, in which homologous points in different strips were compared, and external control, in which the experiments were performed with GCPs, collected by field survey. The results were analysed through six experiments previously mentioned.

The internal quality control will assess the precision of the point cloud, calculating the discrepancies between the coordinates of homologous points in different strips. Owing to the large point spacing achieved by the laser unit used in this study, it is difficult to identify interest points in the cloud since edges and corners are not well-modelled. An alternative to minimise the errors is selecting at least two neighbour points for each interest point in each strip. The coordinates of these points were first collected from point clouds generated without boresight correction (Experiments A and D). Then, their coordinates were recalculated considering each estimated boresight angle set. The statistics such as mean, standard deviation and RMSE (Root Mean Square Error) are calculated from the discrepancies values in two strips. This internal quality control is important to obtain relative errors between strips, mainly caused by system orientation.

The accuracy of the point cloud was estimated in the step of external quality control by computing the discrepancies between the check points coordinates collected in the laser point cloud and the corresponding points measured in the field. The same point collection strategy used in the internal control was repeated in the external quality control. In the external quality control, new statistics are calculated, and the accuracy of the point cloud is analysed based on planimetric and altimetric errors. A second step of the external control analysis refers to the impact of different targets used as control and check points, as well as the development of a strategy to minimise errors in the point-to-point approach using VCP.

5. RESULTS AND DISCUSSION

5.1 Virtual Control Point Assessment

An initial analysis was made regarding the experiments with VCPs by using only the trapezoidal points. The set of interest points was collected in the point cloud without boresight correction and compared the conventional GCPs with the VCPs. A total of 9 points were used to calculate the dispersion measurements, considering that a target could appear in more than one strip. Table 4 presents the RMSE values for the E, N and h coordinates. A slight improvement in the accuracy of the results was observed when using VCPs. The difference of performance when using VCPs (difference of RMSE) in the *N* component is close to 12 cm, and can be explained by the uncertainty in the intersection between planes. Due to the low number and variability of points, the geometry of the planes was not perfectly reconstructed, affecting more significantly the *N* component. However, the results showed an improvement in altimetry, of approximately 37%, in comparison with the experiment with only conventional GCPs. Building corners and centroids of plate targets were discarded in the VCP experiments due to the difficulty in point acquisition.

	GCP	Virtual GCP	Difference of RMSE	Improvement (%)
RMSE E (m)	0.156	0.131	0.025	16%
RMSE N (m)	0.662	0.786	-0.124	-16%
RMSE h (m)	0.243	0.154	0.089	37%

Table 4. Virtual control point performance without boresight correction.

5.2 Assessment of the effects of boresight correction

The results based on relative control from overlapping strips (internal control) are summarised in Table 5. The RMSEs for Experiments from A to F were computed considering seven check points (two trapezoidal, one plate and four building corners). The high magnitude of the error in the *N* component of the point cloud generated without boresight correction (Experiments A and D) suggests a strong influence of the heading angle orientation, which can be affected by the platform alignment. After applying the boresight correction, significant improvements were achieved (Experiments B,C, E and F).

Comparing Experiments C and B with A, there was an improvement of 90.1% and 89.2%, respectively, in the results of the *N* component, which shows that angular misalignment correction is quite significant to LiDAR data collected with UAVs. The results in the planimetric coordinates with boresight angles estimated with the Gauss-Legendre method were slightly better compared to the Gauss-Helmert method.

Experiment F, using boresight angles estimated with Gauss-Helmert adjustment associated with VCP technique, showed improvements compared to the other Experiments, especially in *N* and *h* components. Considering all results, it was observed that the VCP technique was more effective in improving the quality of altimetry. Comparing experiments C and F, which used different weights to the observations with the Gauss-Helmert method, the RMSE of *N* decreased from 0.131 m to 0.104 m and for the h component, from 0.104 m to 0.072 m, an improvement of 20.6% and 30.8%, respectively. The limitation of the experiments in group 2 was the difficulties in using VCPs for entities as plates or building corners, which could improve the results, especially in terms of planimetric coordinates.

Experiments	A	B	C	D	E	F
RMSE E (m)	0.258	0.172	0.184	0.276	0.170	0.179
RMSE N (m)	1.213	0.120	0.131	1.396	0.120	0.104
RMSE h (m)	0.093	0.103	0.104	0.072	0.071	0.072

Table 5. Internal quality control based on a comparison between strips.

The accuracy of the point cloud was assessed with external quality control (Table 6). Comparing Experiments B and C with A, a significant improvement in the accuracy of the planimetric and altimetric coordinates was observed after correcting the systematic errors caused by boresight misalignment, confirming the results shown in the internal quality control. The results obtained with the angles estimated with the Gauss-Helmert method (C) were not significantly better than those achieved with the Gauss-Legendre adjustment method (B). It was expected that the Gauss-Helmert method would estimate the angular misalignments more accurately due to the rigorous observations weighting. It can be seen that the RMSEs were similar for both methods. The RMSE in the *N* component is even slightly larger in experiment C (1.3 cm larger), but small than the measurements errors. The low density of the point cloud, which causes identification errors in the control entities, can explain part of these results. Experiment B had an improvement of

approximately 23.0% for the E component, 81.58% for *N*, and 24.18 % for h, while Experiment C presented improvements of 24.41%, 79.83%, and 23.52%, respectively, compared to Experiment A.

	A	B	C	D	E	F
RMSE E (m)	0.213	0.164	0.161	0.214	0.163	0.162
RMSE N (m)	0.744	0.137	0.150	0.726	0.113	0.105
RMSE h (m)	0.153	0.116	0.117	0.129	0.096	0.094

Table 6. External Quality Control based on check points.

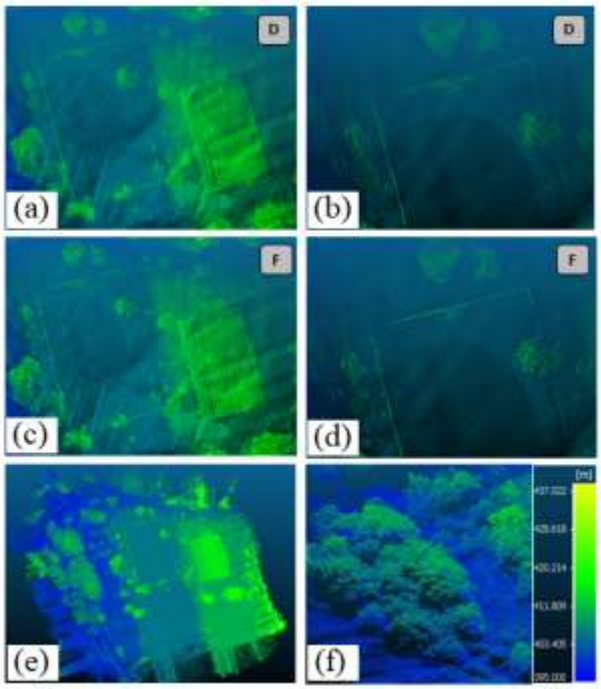

Figure 5. Effects of boresight correction: (a) point cloud without correction, (b) misalignment between strips - fragments of a fence, (c) point cloud with correction, (d) fragment of field fence corrected, (e) top view of a UAV-lidar point cloud of the study area and (f) the 3D view of a fragment of forest.

Considering the experiments using VCPs, improvements were also observed in the accuracy of the results. The RMSE of *N* and *h* decreased from 0.15 m to 0.105 m and from 0.117 m to 0.094 m, respectively, an improvement of 30% and 19.7%. The results for the E component are similar in all the experiments using LSM. Comparing the experiments of group 2, Experiment E had an improvement of approximately 23.8% for E, 84.4% for N, and 25.68% for *h*, while Experiment F presented improvements of 24.3%, 85.5% and 27.1%, respectively, in comparison to Experiment D. The experiments reinforce the importance of correcting the angular misalignment. For the elevations, it was obtained an accuracy of approximately 10 cm for experiments E and F, equivalent to the values presented by Jakkola et al. (2010), Wallace et al. (2011) and Machado et al. (2019). It was observed that no matter the estimation technique (Gauss-Legendre or Gauss-Helmert method) and the type of control, the errors' magnitude in the internal and external control remained similar, but with a slight improvement with the use of the Gauss-Helmert method with virtual GCP.

Figure 5 shows a comparison between point clouds before (Experiment D) and after (Experiment F) boresight correction. In Figure 5.b, a clipping of the point cloud features shows misalignment between overlapping strips. The effect of the correction can be visually identified according to Figure 5.d. In the clipping of the corrected point cloud, the strips are aligned and present high-definition of objects in the scene, such as field fences, trees, corners and building marquees.

The planimetric errors in the check points for Experiments D and F, are depicted in Figure 6. The errors were estimated for five flight strips (1, 2, 3, 4 and 5) according to the North or South flight direction. Strips 1, 3 and 5 were flown in the North direction (represented in blue on the graphic). In experiment D (Figure 6.a), there is a clear trend in the direction which is likely to be caused by non-corrected boresight misalignment angles. In experiment F (Figure 6.b), after boresight correction, it is possible to identify the notable reduction of errors and their random behaviour.

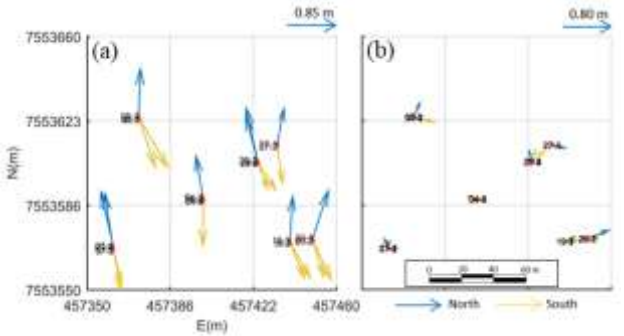

Figure 6. Planimetric errors on GCPs according to strips direction for (a) Experiment D (no boresight correction) and (b) Experiment F (with corrections).

The importance of boresight misalignment correction and virtual point technique is confirmed by the results presented in Table 6, which emphasises the need for these corrections even for lightweight systems onboard UAVs. The final point cloud is presented in Figure 5.e. and f, with an average density of approximately of 11 pts/m², which can be considered suitable for digital agriculture and forest management studies.

6. CONCLUSIONS

This paper presented a case study with the assessment of estimation methods for determining boresight misalignment angles, considering a point-to-point approach. Six experiments were presented in this paper. Regarding the adjustment methods, there were no significant improvements when using the Gauss-Helmert Method in comparison to the Gauss-Legendre Method in this study. These results can be explained by the magnitude of errors from the lightweight system and the difficulties when measuring control points measurements, owing to the low point density. Control points were chosen as control entities because this UAV mapping system was designed for forest management and precision agriculture, where man-made structures, like planes, are not available. Thus, in this kind of environment, it is likely to have artificial targets, like flat panels or trapezoidal 3D targets. Also, to cope with the points sparsity, the VCP was proposed and tested.

The VCP technique is promising, with a slight improvement in performance. Considering the results of the estimation of boresight angles and the final quality control, the results of the technique were more significant when associated with the Gauss-Helmert model. Smaller standard deviations were obtained in the boresight angles estimation and lower RMSE for the *N* and *h* components in the final point cloud. The technique of VCP was tested with trapezoidal control targets. They can be easily assembled in the field, enabling the application of the technique in forest or agriculture monitoring. The final accuracy of the generated point cloud was around 0.19 m in planimetry and 0.094

m in altimetry for the experiment using the Gauss-Helmert method with the VCP approach. Some limitations can be mentioned: (1) the need for special targets or flat surfaces; (2) the minimum number of points for accurate calibration; (3) the knowledge of the raw data and internal errors of the scanning angles which are not usually informed by the manufacturers.

For future works, more experiments with other laser units will be done with further analysis of both estimation methods. In addition, it is important to evaluate the application of the VCP in point clouds with a higher point density. The experiments must also consider the use of this technique with other shapes and comparison with existing calibration strategies.

Considering all the experiments performed, it is emphasised the importance of estimating and correcting of boresight angles in lightweight systems. The Gauss-Helmert, associated with VCP, proved to be a viable alternative for projects with UAV-Lidar systems in areas with a restricted number of well-defined features.

ACKNOWLEDGEMENTS

This study was funded by the Coordenação de Aperfeiçoamento de Pessoal de Nível Superior - Brasil (CAPES) – (Finance Code 88882.433955/2019-01 and 88882.461717/2019-01), the National Council for Scientific and Technological Development – CNPq (Grant: 303670/2018-5) and the São Paulo Research Foundation – FAPESP (Grants: 2013/50426-4 and 2021/06029-7).

REFERENCES

El-Sheimy, N.; Valeo, C.; Habib, A., 2005. Digital Terrain Modeling: Acquisition, Manipulation and Applications, *Artech House*, Norwood, Massachusetts, 257 p.

Elbahnasawy, M., Shamseldin, T., Ravi, R., Zhou, T., Lin, Y. J., Masjedi, A., Habib, A., 2018. Multi-sensor integration onboard a UAV-based mobile mapping system for agricultural management. In *IGARSS 2018-2018 IEEE International Geoscience and Remote Sensing Symposium*, 3412-3415.

Filin, S., 2003. Recovery of systematic biases in LASER altimetry data using natural surfaces. *Photogrammetric Engineering & Remote Sensing*, 69(11), 1235-1242.

Friess, P., 2006. Toward a rigorous methodology for airborne laser mapping. *Proceedings EuroCOW*, 25-27.

Habib, A., Bang, K. I., Kersting, A. P., Chow, J., 2010. Alternative methodologies for LiDAR system calibration. *Remote Sensing*, 2(3), 874-907.

Jaakkola, A., Hyyppä, J., Kukko, A., Yu, X., Kaartinen, H., Lehtomäki, M., Lin, Y., 2010. A low-cost multi-sensoral mobile mapping system and its feasibility for tree measurements. *ISPRS Journal of Photogrammetry and Remote Sensing*, *65*(6), 514-522.

Kersting, A.P.; Habib, A., 2012. A comparative analysis between rigorous and approximate approaches for LiDAR system calibration. *Journal of the Korean Society of Surveying, Geodesy, Photogrammetry and Cartography*, 30(62), 593-605.

Machado, M. D. V., Tommaselli, A. M. G., Torres, F. M., and Campos, M. B., 2019. Postprocessing Synchronization of a Laser Scanning System Aboard a UAV. *Photogrammetric Engineering & Remote Sensing*, 85(10), 753-763.

May, N.C. and Toth, C. K., 2007. Improvement of Lidar Data Accuracy Using Lidar-Specific Ground Targets. *Photogrammetric Engineering & Remote Sensing*, 73(4): 385-396.

May, N. C., 2008. *A rigorous approach to comprehensive performance analysis of state-of-the-art airborne mobile mapping systems*. Doctoral Dissertation. The Ohio State University, 2008.

NOVATEL Inc. SPAN-IGM-S1 Product Sheet. Version 3, 2014. https://hexagondownloads.blob.core.windows.net/public/Novatel/assets/Documents/Manuals/OM-20000141/OM-20000141.pdf

Oliveira Jr, E. M.; Santos, D.R. 2019. Rigorous Calibration of UAV-Based LiDAR Systems with Refinement of the Boresight Angles Using a Point-to-Plane Approach. *Sensors*, 19(23), 5224.

Ojoatre, S., Zhang, C., Hussin, Y. A., Kloosterman, H. E., & Ismail, M. H., 2019. Assessing the uncertainty of tree height and aboveground biomass from terrestrial laser scanner and hypsometer using airborne LiDAR data in tropical rainforests. *IEEE Journal of selected topics in applied earth observations and remote sensing*, 12(10), 4149-4159.

Ravi, R., Lin, Y. J., Elbahnasawy, M., Shamseldin, T., and Habib, A, 2018. Simultaneous system calibration of a multi-lidar multicamera mobile mapping platform. *IEEE Journal of selected topics in applied earth observations and remote sensing*, 11(5), 1694-1714.

RIEGL - Unmanned Scanning, 2023. URL http://www.riegl.com/products/unmanned-scanning/.

Schneider, D. 2009. Calibration of a Riegl LMS-Z420i based on a multi-station adjustment and a geometric model with additional parameters. *Int. Arch. Photogramm. Remote Sens. Spat. Inf*, 38, 177-182,

Štroner, M., Urban, R., Línková, L., 2021. A New Method for UAV Lidar Precision Testing Used for the Evaluation of an Affordable DJI ZENMUSE L1 Scanner. *Remote Sensing* 13, 4811. https://doi.org/10.3390/rs13234811

Shamseldin, T., Ravi, R., Elbahnasawy, M., Lin, Y. J., Habib, A., 2018. Bias Impact Analysis and Calibration of UAV-Based Mobile Lidar System. *In IGARSS 2018-2018 IEEE International Geoscience and Remote Sensing Symposium*, 8769-8772.

Skaloud, J.; Lichti, D.,2006. Rigorous approach to bore-sight self-calibration in airborne laser scanning**.** *ISPRS Journal of Photogrammetry and Remote Sensing*, 61(1), 47-59.

Torres, F. M. and Tommaselli, A. M. G. 2018. A lightweight UAV based laser scanning system for forest application. *Bulletin of Geodetic Sciences*, *24*(3), 318-334.

YellowScan, 2023. Reliable UAV LiDAR systems for Drone 3D laser mapping | YellowScan. URL https://www.yellowscan.com/home/.

Wallace, L., Lucieer, A., Watson, C., Turner, D, 2012. Development of a UAV-LiDAR system with application to forest inventory. *Remote Sensing*, *4*(6), 1519-1543.

Wells, D. E., Krakiwsky, E. J. 1971.*The Method of least squares*. University of New Brunswick.